HHS Public Access

Author manuscript

J Phys Chem C Nanomater Interfaces. Author manuscript; available in PMC 2020 May 09.

Published in final edited form as:

J Phys Chem C Nanomater Interfaces. 2019 May 9; 123(18): 11908–11916. doi:10.1021/acs.jpcc.9b00399.

DNA Translocation through Hybrid Bilayer Nanopores

Ramkumar Balasubramanian[†], **Sohini Pal**[†], **Himanshu Joshi**[‡], **Anjana Rao**[§], **Akshay Naik**[†], **Manoj Varma**[*,†], **Banani Chakraborty**[*,‖], and **Prabal K. Maiti**[*,‡]

[†]Centre for Nano Science and Engineering, Indian Institute of Science, Bangalore 560012, India

[‡]Department of Physics, Indian Institute of Science, Bangalore 560012, India

[§]Division of Signaling and Gene Expression, La Jolla Institute for Allergy and Immunology, La Jolla, California 92037, United States

[‖]Department of Chemical Engineering, Indian Institute of Science, Bangalore 560012, India

Abstract

Pore functionalization has been explored by several groups as a strategy to control DNA translocation through solid-state nanopores. Here we present a hybrid nanopore system consisting of single-layer graphene and a DNA origami layer to achieve base-selective control of DNA translocation rate through aligned nanopores of the two layers. This is achieved by incorporating unpaired dangling bases called overhangs to the origami near the pore region. Molecular dynamics simulations were used to optimize the design of the origami nanopore and the overhangs. Specifically, we considered the influence of the number and spatial distribution of overhangs on translocation times. The simulations revealed that specific interactions between the overhangs and the translocating single-stranded DNA resulted in base-specific residence times.

Graphical Abstract

[*]**Corresponding Authors**: Dr. Banani Chakraborty: banani@iisc.ac.in., Prof. Manoj Varma: mvarma@iisc.ac.in., Prof. Prabal K. Maiti: maiti@iisc.ac.in.

Supporting Information

The Supporting Information is available free of charge on the ACS Publications website at DOI: 10.1021/acs.jpcc.9b00399.

Steps of translocation, translocation times for poly(C)$_{18}$, hydrogen bond formation data for translocating poly-(C)$_{18}$, dynamics of translocation in LS as traps, entanglement of translocating strand with the origami, comparisons between G and A as traps in hybrid nanopore, while poly(T)$_{18}$ translocates, and center of mass calculations. (PDF)

The authors declare no competing financial interest.

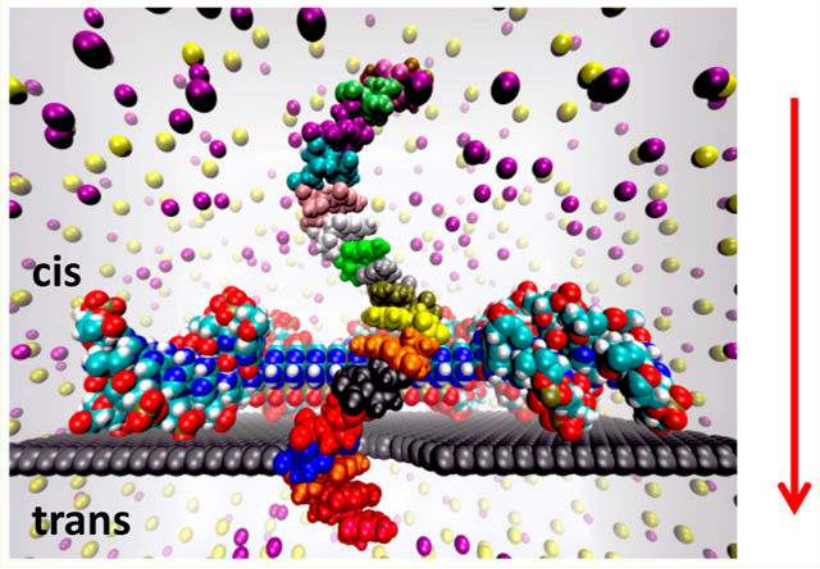

INTRODUCTION

Reliable, cost-effective DNA sequencing is an important and challenging goal with significant promise in the field of healthcare[1,2] due to the strong correlation between the sequence and sequence modifications of disease development and progression.[3] The human genome project has been carried out using the Sanger method,[4] which is time consuming[5] and cost intensive. Nanopore-based single-molecule sequencing techniques have emerged as a highly promising alternative in this direction.[6–9] In this technique, a potential difference (typically 0.1–1 V) is applied across a membrane containing a nanopore (typically 2–20 nm in diameter) causing DNA to be electrophoretically driven through the pore. This process is referred to as DNA translocation. The translocating DNA bases result in the modulation of ionic current passing through the pore, which can potentially be used to identify the translocating base. Nanopore sensors fall into two categories, biological and solid-state nanopores. Translocation of DNA through biological nanopores such as α-hemolysin and MspA has been extensively studied. Biological nanopores are formed by pore-forming proteins, typically a hollow core passing through a mushroom-shaped protein molecule.[10–15] Biological nanopores suffer from variations in pH and ionic strength and lack of long-term stability.[16] Solid-state nanopores are not affected by the pH or ionic strength of sample solutions and offer better control over the pore diameter.[17–19] However, solid-state nanopores have higher noise levels and provide lesser control over translocation of DNA through the pore.[20,21] Monolayer graphene nanopores have been studied extensively for DNA sequencing applications[22–25] due to the close match between single-layer graphene thickness and the distance between two adjacent bases in a DNA strand. The matched spatial dimensions lead to better resolution of ionic current modulations due to the different bases. Extensive molecular dynamics (MD) studies have been done to understand the interactions between the translocating DNA bases and the graphene pore.[26–28] Functionalization of the graphene nanopore, for instance, to control the surface charge, has been explored to slow down DNA[29–31] translocation, which can significantly improve the signal-to-noise ratio and

thereby the base specificity of the measured signal.[32] Spontaneous encapsulation of DNA and RNA inside the nanopore and controlling their translocation time through mechanical force have also been reported.[33,34]

DNA itself can be used for functionalization of solid-state nanopores by virtue of base-pair interactions with the trans-locating strand. DNA origami offers the possibility to fabricate precise nanoscale structures which can be easily integrated with solid-state nanopores for macromolecule[35] sensing as well as to control translocation process.[36,37] Previously, pores made in DNA origami sheets have been combined with glass nanocapillaries for DNA trapping.[38,39] MD studies of the dynamics of DNA origami sheet fluctuations have been done.[40,41] Recently, a graphene–DNA origami hybrid nanopore, consisting of sheets of DNA origami on graphene around the pore, was explored by Farimani et al.[42] for controlling molecular transport through the nanopore system. It was observed that the movement of DNA origami on top of the graphene is effectively decreased owing to the sticky behavior of DNA to graphene, thereby maintaining the initial alignment of the nanopores. They removed bases from the origami sheet near the nanopore to enable a "bait–prey" mechanism[35] for selective control of DNA translocation.

While their work demonstrates the feasibility of such an approach, questions such as effect of number and spatial distribution of the "baits" in selective translocation control have not been addressed so far. In this study, we consider this problem by proposing a different hybrid origami–graphene nanopore system where the geometry of the nanopore and functionality of the baits are decoupled. In other words, the origami contains a nanopore region around which unpaired dangling bases, referred to as overhangs, serve as baits. The number, length, and spatial distribution of the overhangs around the pore control the extent of interaction between the translocating DNA and the hybrid nanopore. The conductivity of the hybrid pores, the residence times of translocating DNA containing different base types, and the mechanism of translocation were investigated in detail.

The main aim of this paper is to study the effect of various pore modifications on base selectivity in DNA sequencing using bait–prey interactions. The sole focus is to optimize the passage and control of single-stranded DNA through the customized nanopore system and how different customizations affect the passage of DNA. This would enable the use of such optimized tailor-made origami sheets to selectively identify bases in experiments. Also, the fabrication of such detection devices to such nanoscale accuracy can be achieved from this hybrid nanopore system that uses DNA origami.

METHODS

Design of the Hybrid Nanopore System.

The DNA origami structures were designed using caDNAno[43] software. The sheet dimensions were 138.6 nm × 114.1 nm × 2 nm with a central pore of size 3.4 nm × 4 nm (Figure 1a). The graphene nanopore underneath this layer had a diameter of 2.1 nm. The relatively larger size of the DNA origami nanopore was to allow for flexibility in the number of overhangs. The PDB (Protein Data Bank) structure was generated from the caDNAno drawing using custom written code written in Nucleic Acid Builder (NAB).[44] The NAB

program generates the bases first and then adds the phosphodiester bonds to get the final intended structure shown in Figure 1a. Simulation was restricted to the pore region of the origami structure for ease of computation as well as because our study primarily focused on the interaction of the overhangs near the pore region with the translocating DNA.

Figure 1b shows the simulated origami sheet whose dimensions are 9.1 nm × 8 nm × 2 nm. Unpaired overhangs were added to the origami staple strands near the pore region. A graphene sheet of 10 nm × 8.5 nm size was generated using a nanotube builder plugin of visual molecular dynamics (VMD).[45] A 2.1 nm pore was created in the graphene sheet, and the DNA origami sheet was placed on top of it with both pores aligned as shown in Figure 1c. In all the simulations, initially three bases of the translocating 18mer ssDNA are inserted into the pore (Figure 1d) to reduce the time involved in searching for the pore entry by the DNA strand.

Different bait configurations were evaluated by varying the length and spatial distribution of the overhangs as shown in Figure 2a. Specifically, we included models with no bait, bait with 2 unpaired bases (henceforth referred to as L2 overhang), and bait with 4 unpaired bases (henceforth referred to as L4 overhang) to each of the 4 corners (Figure 2). In this study, we only considered bait configurations occupying all the corners of the origami pore. In other words, 4 L2 or 4 L4 overhangs were attached to each corner consisting of 8 and 16 (L2:2 × 4 = 8; L4:4 × 4 = 16) total unpaired bases, respectively.

Apart from this, a design with 10 unpaired bases arranged as a strip on either side of the origami pore (henceforth referred to as LS overhang) was also considered (Figure 2c) which had 20 (LS: 2 × 10 = 20) total unpaired bases. The graphene pore of 2.1 nm was chosen which serves as a barrier between the cis and the trans side.

The numbers of baits have not been continuously varied from 0 to an arbitrarily large number as it is computationally expensive. To understand the interactions of overhangs with the translocating DNA, we studied the translocation of 18mer single-stranded poly$(C)_{18}$ and poly$(T)_{18}$ through the pore with either poly A or poly G overhangs in the pore region. For the translocation of the poly$(C)_{18}$ strand, eight designs were made, namely, a system with no origami sheet, an origami sheet with no overhangs, and L2, L4, and LS overhangs with unpaired G and A bases. The same systems were used to study the translocation of the poly$(T)_{18}$ strand. Table 1 provides the complete list of all configurations studied for the translocation studies.

Simulation Methodology.

The initial structure of the origami pore with the graphene sheet and the translocating strand were loaded into the xleap module of AMBER[46] and solvated in a box of TIP3P water. This resulted in simulation boxes with dimensions as shown in Table 1. AMBERff99[47,48] force fields with parmbsc0[49,50] corrections (OL15) were used for describing DNA as they have been reported to reproduce the conformations of large DNA structures.[51] Joung–Cheatham ion parameters[52] were used for describing the interaction of the ions in the system. Particle mesh Ewald (PME)[53] was used to calculate long-range electrostatic interactions, and a cutoff of 9 Å was used for short-range interactions. The SHAKE[54] algorithm was used to

restrain all the bonds involving hydrogen and allowed us to use an integration time step of 2 fs. The origami and the graphene sheets were initially harmonically restrained to 500 kcal/mol $Å^{-2}$. To remove the bad contacts, the system was subjected to energy minimization which involved 3000 steps of steepest descent and 1000 steps of conjugate gradient while slowly reducing the harmonic restraint to zero. After the energy minimization, 40 ps of MD simulation was performed with an integration time step of 1 fs. During MD, the system was gradually heated from 0 to 300 K with the origami and the graphene harmonically restrained to their starting configuration using a force constant of 20 kcal/mol $Å^{-2}$. Subsequently, equilibration of the system under constant pressure–constant temperature conditions (NPT) was performed which consisted of the following steps: (a) equilibration with a harmonic restraint of 1 kcal/mol $Å^{-2}$ for 1 ns; (b) equilibration with a harmonic restraint of 0.5 kcal/mol $Å^{-2}$ for 0.5 ns; and (c) equilibration with no restraint for 25 ps. The Berendsen weak coupling method[55] was used for both the temperature and pressure regulation with 0.5 ps time constant for a heat bath coupling and 0.5 ps pressure relaxation time. For translocation simulations, 5 kcal/mol $Å^{-2}$ harmonic restraint was applied to the outer corners of the origami sheet and also to the carbon atoms inside a ring of 2 nm radius around the pore. The system was solvated in 1 M NaCl solution. The rest of the carbon atoms of the graphene sheet were fixed.

A constant electric field was applied along the Z direction (Figure 2g) and was calculated from the voltage difference across the membrane as $V = -El_{\text{trans}}$ (l_{trans} is the length of the system box along the translocation axis), and translocation simulations were performed using NAMD[56] with AMBER force field parameters. The ionic current was computed by $I(t) = \frac{\sum_{i=1}^{N} q_i\left[z_i(t+\Delta t) - z_i(t)\right]}{\Delta t L_z}$, where N represents the total number of charge carriers contributing to the ionic current; Δt is the sampling frequency (10 ps); $z_i(t+\Delta t)$ and $z_i(t)$ represent the z coordinate of the ith ion within the Δt; and q_i represents the charge of the ion. The graphical visualization presented in this study and analysis of the data were done using custom scripts written in VMD and the CPPTRAJ software module of AMBER14.[57]

RESULTS AND DISCUSSIONS

Pore Characteristics.

The conductivity of hybrid nanopores with origamis containing different bait configurations was computed. To understand the effect of the origami and baits on the nanopore conductivity, we compute the ionic current for different applied voltages. I–V characteristics for different origami designs are shown in Figure 3(a). The simulations were run for 40 ns, and the ionic current value was block averaged over the entire simulation time. It was observed that though the ions pass through the porous DNA origami sheet they are hindered by the graphene layer. The translocating strands were not included in the simulation for computing the pore conductivity. The conductance was extracted from a linear fit of the I–V characteristic curve (Figure 3b). The conductance values extracted from the simulations were 2.99 nS (bare graphene nanopore), 2.81 nS (origami without baits, refer to Table 1 for nomenclature of the origami types), 2.51 nS (G2 origami, L2 with unpaired G bases), 2.13 nS (G4 origami, L4 with unpaired G bases), and 2.29 nS (GS origami, LS with unpaired G

bases). The conductance of the bare graphene nanopore and that of the system with the origami on the graphene sheet without the baits are qualitatively very similar. However, the presence of unpaired bases from the baits impedes the ionic current. Consequently, the G4 exhibits a lower conductance compared to G2, which in turn had a conductance lower than an origami with no baits. In the case of GS, despite the higher number of unpaired bases, the spatial organization of the unpaired bases makes them less flexible than that of G4. The mean variance of center of masses (σ^2_{COM}) of the unpaired bases in G4 and GS was computed and was found to be 16.91 $Å^2$ and 9.69 $Å^2$, respectively, for a potential difference of 2 V (see section S1 of Supporting Information). This quantitatively establishes the reduced degrees of freedom of the baits in GS despite having more unpaired bases.

As a result, the GS conductance was slightly higher than the G4 value but smaller than G2. To understand the effect of the applied bias in the translocation process, we have also calculated the instantaneous electrostatic potential map (averaged over the entire simulation time) under an applied bias of 2 V, and it is shown in Figure 3c and 3d. The electrostatic potential near the pore region is slightly modified because of the presence of DNA origami. For the calculation of the potential the point charges were approximated by Gaussian spheres[58] with an inverse width of $\beta = 0.25$ $Å^{-1}$. The change in the potential profile is more for the case with a strip of overhangs than with no overhangs. We also average the potential along the *x* and *y* direction and plot the total electrostatic potential along the direction of the applied bias which is along the *z*-direction. We find a sharp drop in the potential across the graphene nanopore and almost a constant potential across the DNA origami region. Note that similar behavior was seen in the study by Farimani et al.[42] It is seen that most of the potential drop is near the graphene nanopore (Figure 3e), and the type of origami did not significantly affect the potential distribution. A magnified view of the potential distribution near the nanopore is shown in Figure 3f. The pore ionic selectivity studies were not done at negative biases. Applying negative voltages would cause detachment of the origami from the graphene substrate.[42]

ssDNA Translocation Studies.

To understand the trans-location of ssDNA (single-stranded DNA) through the hybrid nanopore, a bias of 2 V was applied along the z axis. The choice of 2 V is to ensure faster computational time. Eight independent trials for each configuration were run. The base is defined to have translocated when its distance along the axis of the applied electric field exceeds 3.4 Å from the graphene base. Initially, three bases are inside the pore, and so the translocation times that are calculated are effectively for 15 bases. We illustrate the role of the origami and the baits by taking the example of translocation of a ssDNA sequence $poly(C)_{18}$. $Poly(C)_{18}$ translocates across a bare graphene nanopore in a time scale of 2–4 ns, which increases to 7–9 ns on addition of the origami sheet without baits on top of graphene. This is expected due to the increased molecular interactions between the bases in the origami sheet and the translocating strand as seen in Figure 4.

Addition of baits to the origami resulted in further increase in translocation times due to base-specific interactions between the translocating $poly(C)_{18}$ strand and the unpaired G bases in the bait region. The average translocation times for $poly(C)_{18}$ in G2, G4, and GS

were 12.09 ns, 55.43 ns, and 108.21 ns, respectively, in line with the increased number of unpaired bases in the bait to interact with the translocating ssDNA. The translocation times for the different configurations studied are provided in Table 2.

As expected, changing the unpaired bases from G to A reduced the translocation time of the poly$(C)_{18}$ strand due to lack of base complementarity between the translocating strand and the bait. The average translocation times for A2, A4, and AS were 10.35 ns, 28.61 ns, and 15.67 ns, respectively. As the conductance of L4 is less than LS (Figure 3b) in the absence of complementary interactions between translocating strands and the baits, translocation should happen faster in LS compared to L4 which explains a higher mean translocation time for A4 when compared to AS. These results clearly show that incorporating appropriate bait had a remarkable effect on the translocation time which exhibited an increasing trend with the increase in number of unpaired complementary bases in the bait region of the origami.

To further confirm that the increase in translocation time is due to complementary base–pair interactions between the translocating strand and the bait region, we investigated the number of hydrogen bonds formed during the translocation (Figure 5). It was seen that the number of hydrogen bonds correlated with the residence time of the bases during translocation. In other words, an increased number of hydrogen bonds was indicative of slower translocation.

This was true only when the translocating strand was complementary to the bait region as seen in Table 2. Changing the bait region to unpaired A's, not complementary to the translocating poly$(C)_{18}$, resulted in a 7 times decrease in the rate of hydrogen bond formation from ~42 bonds/ns to ~6 bonds/ns for the LS overhangs (more information in Table S2). The rate of hydrogen bond formation is the total number of hydrogen bonds formed during the complete translocation process divided by the translocation time. The statistics of hydrogen bond formation between specific and nonspecific bait–target interaction is shown in Figure 5a and 5b. Further evidence of specific base–pair interactions is obtained when the dynamics of motion of the translocating strand is analyzed for the LS system. Figure 5c shows that the center of mass of translocating poly$(C)_{18}$ is very close to that of one of the arms of the GS overhang, presumably due to specific C–G interaction. On the other hand, no such bias is observed when the overhang is composed of nonspecific A bases. (Dynamics shown in Table S3.) Figure 6 shows the per base translocation times for A4, AS, G4, and GS.

Translocation of poly$(T)_{18}$ was also studied in exactly the same manner as described above for poly$(C)_{18}$. The results are summarized in Table S3 (Supporting Information) where it can be seen that the translocation behavior shows exactly similar trends as those of poly$(C)_{18}$. All these observations taken together provide confidence of our hypothesis that specific base–pair interactions strongly determine the translocation dynamics in our system.

DISCUSSION AND OPEN QUESTIONS

Although the results shown in the previous section illustrate the role of specific base interactions between the translocating strand and the unpaired bases of the overhangs, here we discuss some other factors which also affect the translocation behavior. In particular, we

discuss the role of substrate interactions with the translocating strand and conformational flexibility of the baits in the bait–prey system on the translocation dynamics.

Some of the poly$(C)_{18}$ translocation events were found to be unusually long, particularly with G4 and GS overhangs. These have been indicated in red font in Supporting Information Table S1. We found that such large residence times were caused due to the interaction of the translocating strand with the graphene substrate. An example of such an event is shown in the image sequence S1 (Supporting Information Figure S1). Figure S1(f) shows the translocating strand sticking to the graphene substrate on the trans side. Such events highlight the crucial role of DNA–substrate interactions in the observed translocation behavior in our system. For instance, it is possible that slowing down of the translocating strand due to stiction on graphene may enhance the rate of bait–prey interactions between the translocating strand and the origami. Vice versa, enhanced bait–prey interactions may also increase interactions between the translocating strand and the substrate for the same reason. We are currently exploring an origami–nanopore system which can separate out bait–prey interactions from the substrate interactions. Such studies will elucidate the role of the substrate in translocation behavior in our system.

As pointed out earlier, the conductance of GS overhangs turns out to be larger than that of G4, in spite of a larger number of unpaired bases in GS. This implies that the number of bases alone is not sufficient to understand conductance as well as translocation dynamics through the nanopore. In addition to the number of unpaired bases, the flexibility of motion of the unpaired bases also appears to be an important factor. Analysis of the motion of unpaired bases revealed that LS is less flexible than L4 (Figure S3 Supporting Information). This analysis is also supported by the observation that the translocation times for the noncomplementary strand were significantly higher for the L4 strand compared to the LS strand. Translocation of the noncomplementary strand should not be significantly affected by the number of unpaired bases due to the lack of specific base–pair interactions. Therefore, any difference in the translocation of the noncomplementary strand should come from stochastic, nonspecific base–pair interactions. Increased flexibility of the unpaired bases in the overhangs enhances the chance of such stochastic interactions which we believe leads to increased translocation times of the noncomplementary strand translocating through L4 compared to LS. Further, in the case of a complementary strand translocation, the increase in trans-location time for LS is nearly 2× that of L4, while the number of unpaired bases is only 25% larger. This observation is also strongly suggestive of the role of conformational flexibility of unpaired bases employed in a bait–prey system such as ours. A major challenge in this hybrid nanopore system is fabrication of the aligned DNA origami and graphene pores. An important aspect of our design is that it is the DNA origami structure which is responsible for selectivity. The graphene substrate serves as a support to the origami sheet, and therefore extremely precise alignment between the two pores is not critical. From our own experimental data as well as other reports in the literature, it is possible to align the pores of an origami sheet and an underlying solid-state membrane by simply allowing the origami to dock onto the solid-state membrane under the action of a potential applied across the membrane. For large nanopores >10 nm, this works well in practice. However, aligning 1–2 nm diameter nanopores in the origami and a graphene sheet may not be perfect using

this method. It is possible to use thiol-modified strands on the origami to dock to gold nanodots on the graphene sheet to increase alignment tolerance.[59,60]

CONCLUSIONS

In summary, we have simulated the translocation of ssDNA through a hybrid graphene origami and demonstrated that the design of the origami pore results in tailoring the selectivity of the pore. Different origami pore designs on graphene were evaluated for their effect on translocation of complementary and noncomplementary strands. It was found that complementary interactions between the translocating strand and unpaired bases (baits) in the origami resulted in significantly longer translocation time correlating with increased rate of hydrogen bond formation. While this was expected, we also found evidence for the role of substrate–DNA interactions and conformational flexibility of the baits in determining translocation behavior. Our studies provide insight into optimal design of hybrid DNA origami nanopore structures for sensing and sequencing.

Supplementary Material

Refer to Web version on PubMed Central for supplementary material.

ACKNOWLEDGMENTS

We acknowledge Supercomputer Education and Research Centre, (SERC) IISc Bangalore, for providing access to the high-performance supercomputer SahasraT. R.K. and S.P. thank MHRD, GoI, for research fellowship. We also acknowledge the use of facilities at Centre for Nano Science and Engineering, Indian Institute of Science, Bangalore, India. Banani Chakraborty thanks the Ramalingaswami fellowship from DBT, GoI.

REFERENCES

(1). Shendure J; et al. Dna Sequencing At 40: Past, Present and Future. Nature 2017, 550, 345–353. [PubMed: 29019985]

(2). Goodwin S; McPherson JD; McCombie W Coming Of Age: Ten Years Of Next-Generation Sequencing Technologies. Nat. Rev. Genet 2016, 17, 333–351. [PubMed: 27184599]

(3). Levinson DF The Genetics Of Depression: A Review. Biol. Psychiatry 2006, 60, 84–92. [PubMed: 16300747]

(4). Sanger F; Nicklen S; Coulson AR Dna Sequencing With Chain-Terminating Inhibitors. Proc. Natl. Acad. Sci. U. S. A 1977, 74, 5463–5467. [PubMed: 271968]

(5). Beck TF; Mullikin JC NISC Comparative Sequencing Program, on behalf of the N. C. S. & Biesecker, L. G. Systematic Evaluation Of Sanger Validation Of Next-Generation Sequencing Variants. Clin. Chem 2016, 62, 647–654. [PubMed: 26847218]

(6). Venkatesan BM; Bashir R Nanopore Sensors For Nucleic Acid Analysis. Nat. Nanotechnol 2011, 6, 615–624. [PubMed: 21926981]

(7). Lansac Y; Maiti PK; Glaser MA Coarse-Grained Simulation Of Polymer Translocation Through An Artificial Nanopore. Polymer 2004, 45, 3099–3110.

(8). Deamer DW; Branton D Characterization Of Nucleic Acids By Nanopore Analysis. Acc. Chem. Res 2002, 35, 817–825. [PubMed: 12379134]

(9). Keyser UF Controlling Molecular Transport Through Nanopores. J. R. Soc., Interface 2011, 8, 1369–1378. [PubMed: 21715402]

(10). Kasianowicz JJ; Brandin E; Branton D; Deamer DW Characterization Of Individual Polynucleotide Molecules Using A Membrane Channel. Proc. Natl. Acad. Sci. U. S. A 1996, 93, 13770–13773. [PubMed: 8943010]

(11). Akeson M; Branton D; Kasianowicz JJ; Brandin E; Deamer DW Microsecond Time-Scale Discrimination Among Polycytidylic Acid, Polyadenylic Acid, and Polyuridylic Acid As Homopolymers Or As Segments Within Single Rna Molecules. Biophys. J 1999, 77, 3227–3233. [PubMed: 10585944]

(12). Cockroft SL; Chu J; Amorin M; Ghadiri MR; Ghadiri MR A Single-Molecule Nanopore Device Detects Dna Polymerase Activity With Single-Nucleotide Resolution. J. Am. Chem. Soc 2008, 130, 818–820. [PubMed: 18166054]

(13). Derrington IM; et al. Nanopore Dna Sequencing With MSPA. Proc. Natl. Acad. Sci. U. S. A 2010, 107, 16060–16065. [PubMed: 20798343]

(14). Manrao EA; et al. Reading Dna At Single-Nucleotide Resolution With A Mutant MSPA Nanopore and PHI29 Dna Polymerase. Nat. Biotechnol 2012, 30, 349–353. [PubMed: 22446694]

(15). Kumar H; Lansac Y; Glaser MA; Maiti PK Biopolymers In Nanopores: Challenges And Opportunities. Soft Matter 2011, 7, 5898–5907.

(16). Haque F; Li J; Wu H-C; Liang X-J; Guo P Solid-State and Biological Nanopore For Real-Time Sensing Of Single Chemical And Sequencing Of Dna. Nano Today 2013, 8, 56–74. [PubMed: 23504223]

(17). Storm AJ; Chen JH; Ling XS; Zandbergen HW; Dekker C Fabrication Of Solid-State Nanopores With Single-Nanometre Precision. Nat. Mater 2003, 2, 537–540. [PubMed: 12858166]

(18). Venkatesan BM; et al. Highly Sensitive, Mechanically Stable Nanopore Sensors For Dna Analysis. Adv. Mater 2009, 21, 2771–2776. [PubMed: 20098720]

(19). Kim MJ; Wanunu M; Bell DC; Meller A Rapid Fabrication Of Uniformly Sized Nanopores and Nanopore Arrays For Parallel Dna Analysis. Adv. Mater 2006, 18, 3149–3153.

(20). Branton D; et al. The Potential and Challenges Of Nanopore Sequencing. Nat. Biotechnol 2008, 26, 1146–1153. [PubMed: 18846088]

(21). Iqbal SM; Akin D; Bashir R Solid-State Nanopore Channels With Dna Selectivity. Nat. Nanotechnol 2007, 2, 243–248. [PubMed: 18654270]

(22). Geim AK Graphene: Status and Prospects. Science 2009, 324, 1530–1534. [PubMed: 19541989]

(23). Fischbein MD; Drndić M Electron Beam Nanosculpting Of Suspended Graphene Sheets. Appl. Phys. Lett 2008, 93, 113107–113103.

(24). Merchant CA; et al. Dna Translocation Through Graphene Nanopores. Nano Lett. 2010, 10, 2915–2921. [PubMed: 20698604]

(25). Schneider GF; Dekker C Dna Sequencing With Nanopores. Nat. Biotechnol 2012, 30, 326–328. [PubMed: 22491281]

(26). Wells DB; Belkin M; Comer J; Aksimentiev A Assessing Graphene Nanopores For Sequencing Dna. Nano Lett. 2012, 12, 4117–4123. [PubMed: 22780094]

(27). Qiu H; Sarathy A; Leburton JP; Schulten K Intrinsic Stepwise Translocation Of Stretched Ssdna In Graphene Nanopores. Nano Lett. 2015, 15, 8322–8330. [PubMed: 26581231]

(28). Sathe C; Zou X; Leburton J-P; Schulten K Computational Investigation Of Dna Detection Using Graphene Nanopores. ACS Nano 2011, 5, 8842–8851. [PubMed: 21981556]

(29). Banerjee S; et al. Slowing Dna Transport Using Graphene-Dna Interactions. Adv. Funct. Mater 2015, 25, 936–946. [PubMed: 26167144]

(30). Luan B; Stolovitzky G; Martyna G Slowing and Controlling The Translocation Of Dna In A Solid-State Nanopore. Nanoscale 2012, 4, 1068–77. [PubMed: 22081018]

(31). Sint K; Wang B; Kral P Selective Ion Passage Through Functionalized Graphene Nanopores. J. Am. Chem. Soc 2008, 130, 16448–16449. [PubMed: 19554715]

(32). Yu Y; Lu X; Ding H; Ma Y Computational Investigation On Dna Sequencing Using Functionalized Graphene Nanopores. Phys. Chem. Chem. Phys 2018, 20, 9063–9069. [PubMed: 29446423]

(33). Sahoo AK; Kanchi S; Mandal T; Dasgupta C; Maiti PK Translocation Of Bioactive Molecules Through Carbon Nanotubes Embedded In The Lipid Membrane. ACS Appl. Mater. Interfaces 2018, 10, 6168–6179. [PubMed: 29373024]

(34). Mogurampelly S; Maiti PK Translocation and Encapsulation Of Sirna Inside Carbon Nanotubes. J. Chem. Phys 2013, 138, 034901. [PubMed: 23343299]

(35). Wei R; Martin TG; Rant U; Dietz H Dna Origami Gatekeepers For Solid-State Nanopores. Angew. Chem., Int. Ed 2012, 51, 4864–4867.

(36). Winfree E; Liu F; Wenzler LA; Seeman NC Design and Self-Assembly Of Two-Dimensional Dna Crystals. Nature 1998, 394, 539–544. [PubMed: 9707114]

(37). Rothemund PWK Folding Dna To Create Nanoscale Shapes and Patterns. Nature 2006, 440, 297–302. [PubMed: 16541064]

(38). Hernandez-Ainsa S; et al. Dna Origami Nanopores for Controlling Dna Translocation. ACS Nano 2013, 7, 6024–6030. [PubMed: 23734828]

(39). Keyser UF Enhancing Nanopore Sensing With Dna Nanotechnology. Nat. Nanotechnol 2016, 11, 106–108. [PubMed: 26839252]

(40). Yoo J; Aksimentiev A In Situ Structure And Dynamics Of Dna Origami Determined Through Molecular Dynamics Simulations. Proc. Natl. Acad. Sci. U. S. A 2013, 110, 20099–104. [PubMed: 24277840]

(41). Li C-Y; et al. Ionic Conductivity, Structural Deformation, and Programmable Anisotropy Of Dna Origami In Electric Field. ACS Nano 2015, 9, 1420–1433. [PubMed: 25623807]

(42). Barati Farimani A; Dibaeinia P; Aluru NR Dna Origami–Graphene Hybrid Nanopore For Dna Detection. ACS Appl. Mater. Interfaces 2017, 9, 92–100. [PubMed: 28004567]

(43). Douglas SM; et al. Rapid Prototyping Of 3d Dna-Origami Shapes With Cadnano. Nucleic Acids Res. 2009, 37, 5001–5006. [PubMed: 19531737]

(44). Macke TJ; Case DA Modeling Unusual Nucleic Acid Structures. Molecular Modeling of Nucleic Acids, ACS Symposium Series 1997, 682, 379–393.

(45). Humphrey W; Dalke A; Schulten K Vmd: Visual Molecular Dynamics. J. Mol. Graphics 1996, 14, 33–38.

(46). Case DA; et al. The Amber Biomolecular Simulation Programs. J. Comput. Chem 2005, 26, 1668–1688. [PubMed: 16200636]

(47). Cornell WD; et al. A Second Generation Force Field For The Simulation Of Proteins, Nucleic Acids, and Organic Molecules. J. Am. Chem. Soc 1995, 117, 5179–5197.

(48). Cheatham TE; Cieplak P; Kollman PA A Modified Version Of The Cornell Et Al. Force Field With Improved Sugar Pucker Phases And Helical Repeat. J. Biomol. Struct. Dyn 1999, 16, 845–862. [PubMed: 10217454]

(49). Pérez A; et al. Refinement Of The Amber Force Field For Nucleic Acids: Improving The Description of α/γ Conformers. Biophys. J 2007, 92, 3817–3829. [PubMed: 17351000]

(50). Dans PD; et al. How Accurate Are Accurate Force-Fields For B-Dna? Nucleic Acids Res. 2017, 45, 4217–4230. [PubMed: 28088759]

(51). Maiti PK; Pascal TA; Vaidehi N; Goddard WA The Stability Of Seeman Jx Dna Topoisomers Of Paranemic Crossover (Px) Molecules As A Function Of Crossover Number. Nucleic Acids Res. 2004, 32, 6047–6056. [PubMed: 15550565]

(52). Joung IS; Cheatham TE Determination Of Alkali And Halide Monovalent Ion Parameters For Use In Explicitly Solvated Bio-molecular Simulations. J. Phys. Chem. B 2008, 112, 9020–9041. [PubMed: 18593145]

(53). Darden T; York D; Pedersen L Particle mesh Ewald: An N LOG(N) Method For Ewald Sums In Large Systems. J. Chem. Phys 1993, 98, 10089–10092.

(54). Ryckaert J-P; Ciccotti G; Berendsen HJ Numerical Integration Of The Cartesian Equations Of Motion Of A System With Constraints: Molecular Dynamics Of N-Alkanes. J. Comput. Phys 1977, 23, 327–341.

(55). Berendsen HJC; Postma JPM; van Gunsteren WF; DiNola A; Haak JR Molecular Dynamics With Coupling To An External Bath. J. Chem. Phys 1984, 81, 3684–3690.

(56). Phillips JC; et al. Scalable Molecular Dynamics With NAMD. J. Comput. Chem 2005, 26, 1781–1802. [PubMed: 16222654]

(57). Roe DR; Cheatham TE PTRAJ And CPPTRAJ: Software For Processing And Analysis Of Molecular Dynamics Trajectory Data. J. Chem. Theory Comput 2013, 9, 3084–3095. [PubMed: 26583988]

(58). Aksimentiev A; Schulten K Imaging α-Hemolysin With Molecular Dynamics: Ionic Conductance, Osmotic Permeability, And The Electrostatic Potential Map. Biophys. J 2005, 88, 3745–3761. [PubMed: 15764651]

(59). Bell NAW; et al. Dna Origami Nanopores. Nano Lett. 2012, 12, 512–517. [PubMed: 22196850]

(60). Ding B; et al. Interconnecting Gold Islands With Dna Origami Nanotubes. Nano Lett. 2010, 10, 5065–5069. [PubMed: 21070012]

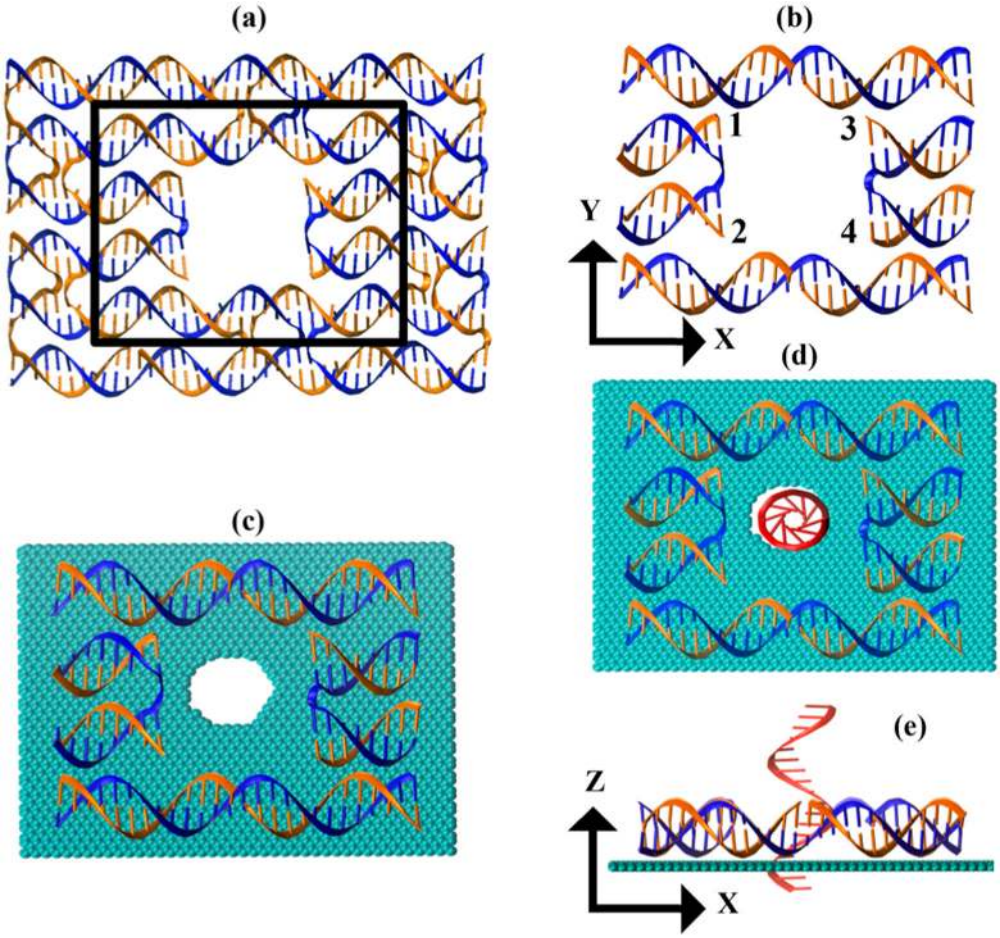

Figure 1.

(a) Generated origami sheet. (b) The segment used for all atom fine grain MD simulations showing the origami sheet without overhangs (scaffold in blue). Overhangs are added to the four points in the staple strands (denoted by numbers). (c) Origami sheet on top of the graphene sheet with their pores aligned. (d) Top and (e) side view of the system with translocating DNA (in red).

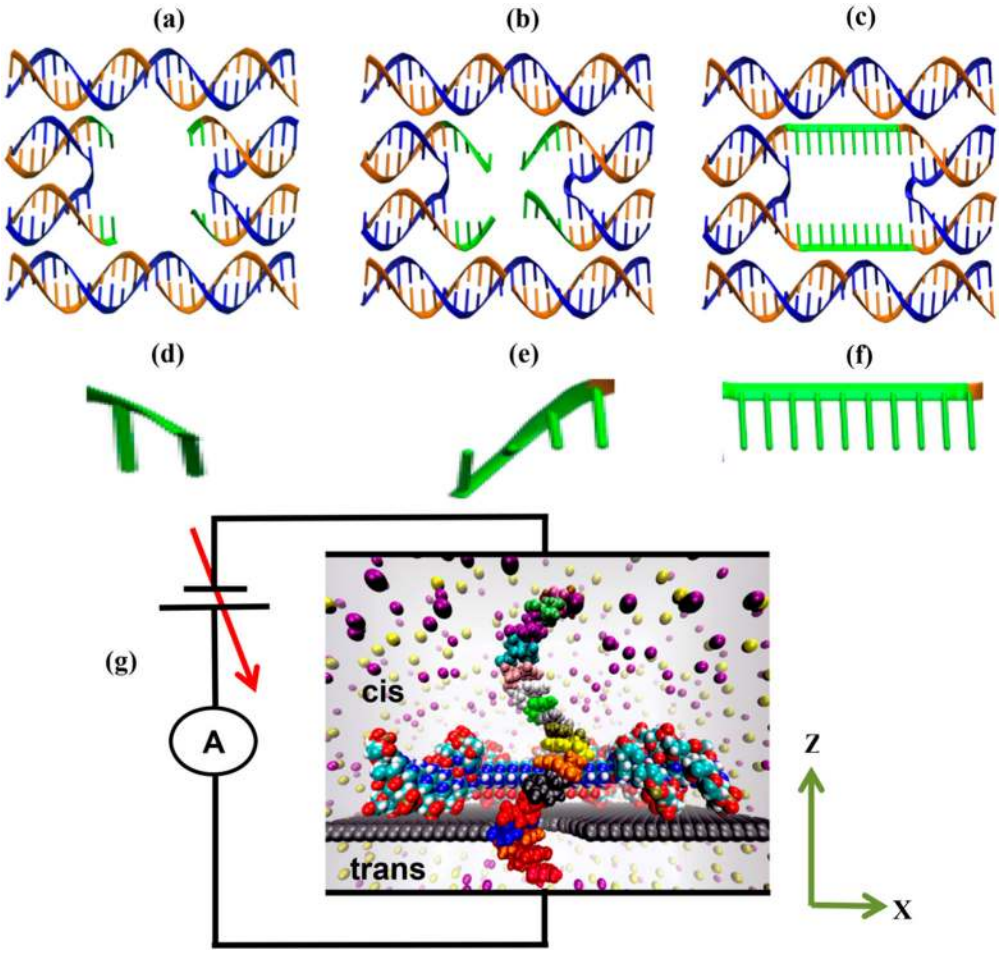

Figure 2.

(a) Origami sheet with 4 × L2 overhangs (8 unpaired bases), (b) 4 × L4 overhangs on each corner (16 unpaired bases), and (c) origami with 2 × LS (20 unpaired bases). All the unpaired bases are shown in green. (d–f) Single L2, L4, and LS overhangs having 2, 4, and 10 unpaired bases, respectively. (g) Cross-section along the x–z plane showing the hybrid nanopore with ions and the translocating DNA in a water box.

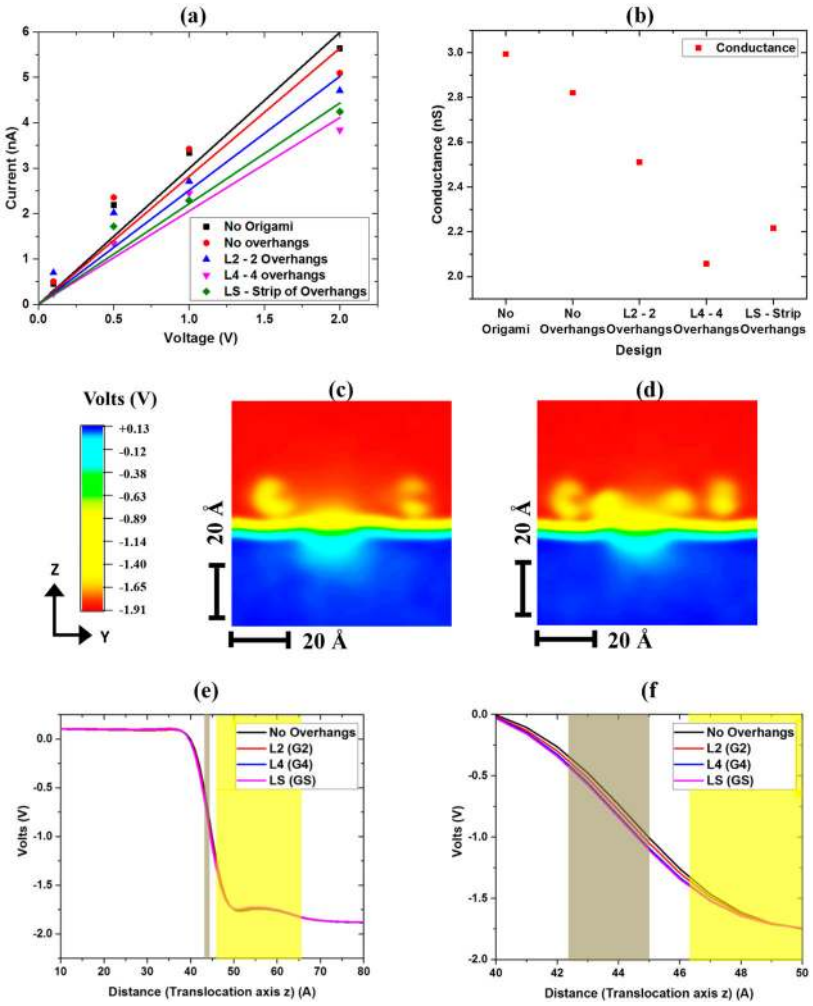

Figure 3.

(a) I–V characteristics of different pore systems with linear fits corresponding to the respective colors. (b) Conductance in nS for different designs. Electrostatic potential maps (applied voltage 2 V) for (c) hybrid nanopore with no overhangs in the origami sheet and (d) strip of overhangs in the sheet (2 × LS). (e) Comparison of mean bias along the *z* axis after averaging over the *x* and *y* axes for different hybrid nanopore designs. Brown: graphene layer; Yellow: Origami sheet. (f) The change in potential around the graphene sheet is zoomed in. It shows almost a similar drop in potential for all the systems.

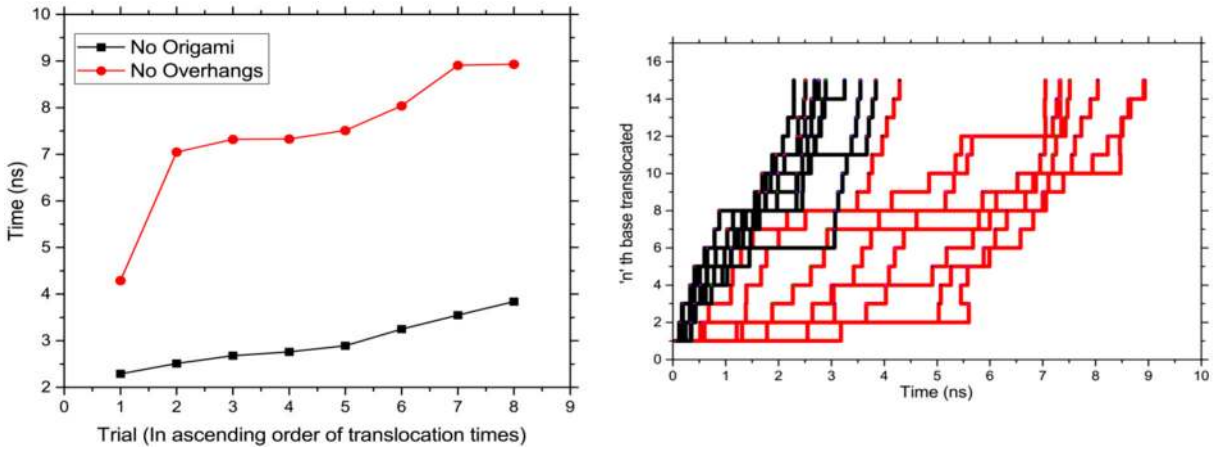

Figure 4.

(a) Comparison of translocation times for designs with no origami and design with origami having no overhangs. The trials have been plotted in the ascending order of their translocation times. (b) Base by base translocation for both the design with all the trials included (Black: Data for the case with no origami; Red: Data with the case for Design of Origami sheet without overhangs).

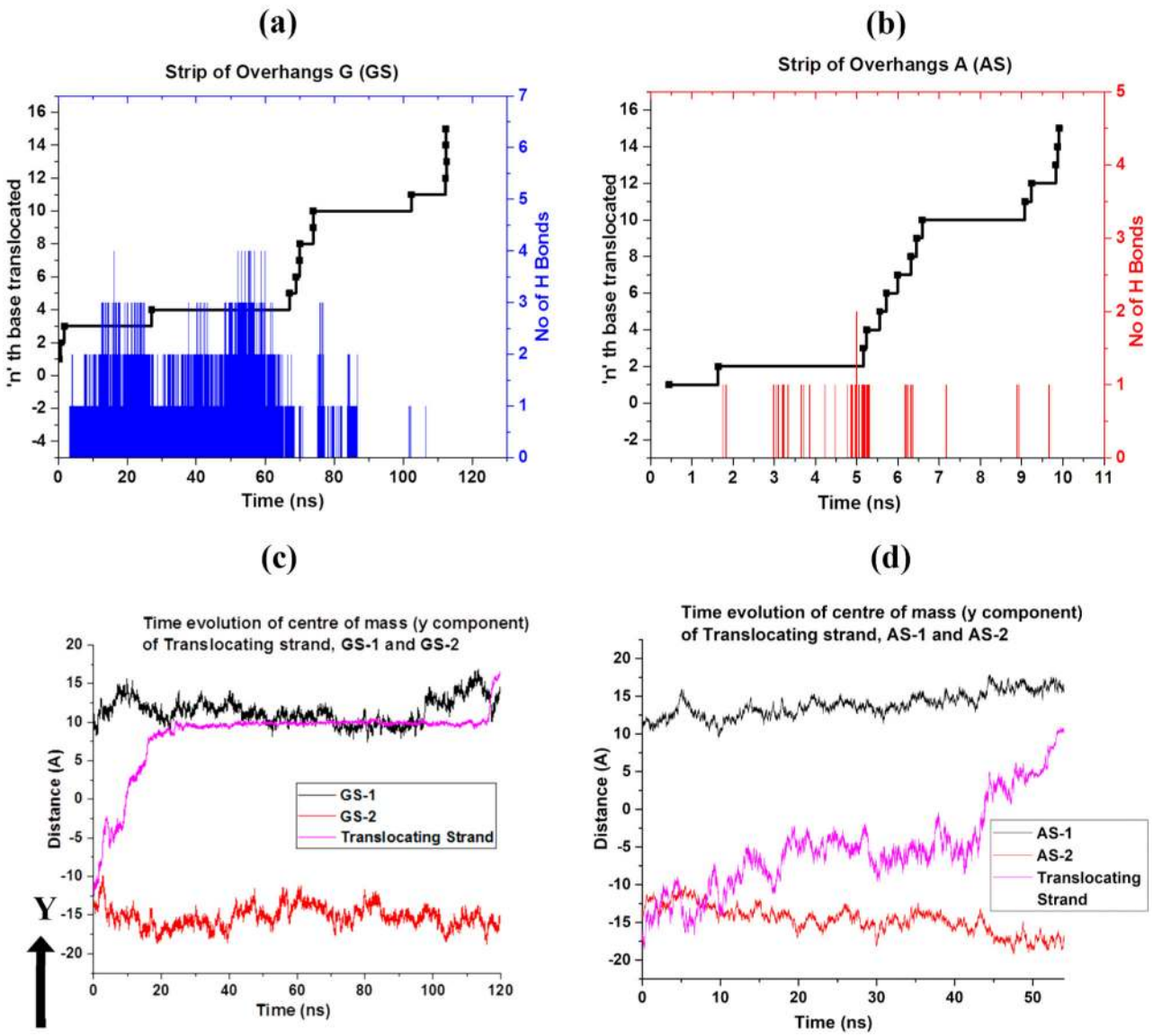

Figure 5.

H bonds formed between translocating strand and the overhangs. (a) G-strip vs polyC-18. More hydrogen bonds are seen to be formed as the bases are complementary. (b) G-strip vs polyC-18. Less hydrogen bond formation is observed. (c) Time evolution of the *y*-component of center of masses of GS1, GS2, and translocating strand. (d) Time evolution of the y-component of center of masses of AS1, AS2, and translocating strand.

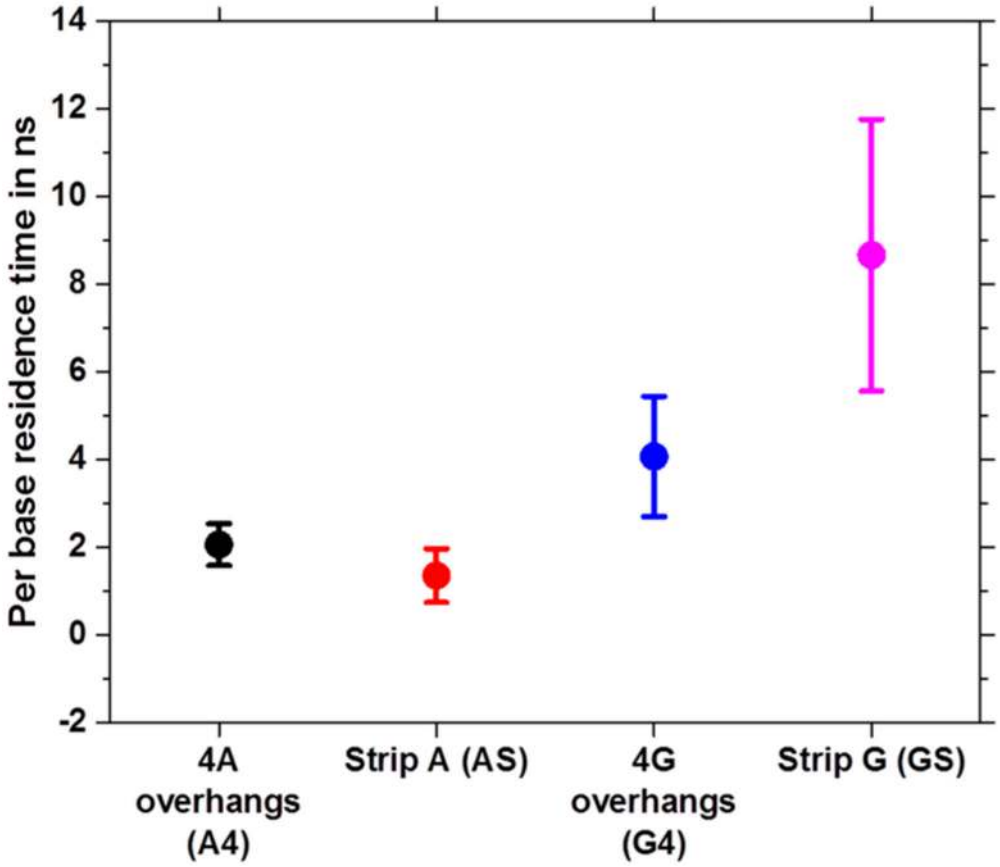

Figure 6.

Comparison of per base translocation times of polyC-18 in A-4, A-strip, G-4, and G-strip nanopore models ($p = 0.027$ for 4A vs 4G; $p = 0.00034$ for AS vs GS; $p = 0.03387$ for 4G vs GS).

Table 1.

Simulated Models for Translocation Studies Denoting Translocating Strands and Overhang Bases

translocating strand	origami sheet design		overhang bases	number of atoms	box dimensions *[X Y Z]* (Å)	
poly(C)$_{18}$	no origami (only graphene)		--	90644	[107 94 108]	
	origami sheet	No baits	--	86088	[107 92 108]	
		2 overhangs (G2)	poly G	86099	[107 92 108]	
		4 overhangs (G4)		85972	[107 92 108]	
			strip of overhangs (GS)		87497	[107 94 108]
		2 overhangs (A2)	poly A	85962	[107 92 108]	
		4 overhangs (A4)		85962	[107 92 108]	
		strip of overhangs (AS)		87468	[107 94 108]	
poly(T)$_{18}$	no origami (only graphene)		--	89343	[107 92 108]	
	origami sheet	no baits	--	86352	[107 92 108]	
		2 overhangs(A2)	poly A	86163	[107 92 108]	
		4 overhangs (A4)		86073	[107 92 108]	
		strip of overhangs (AS)		87591	[107 94 108]	
		2 overhangs (G2)	poly G	86201	[107 92 108]	
		4 overhangs (G4)		86089	[107 92 108]	
		strip of overhangs (GS)		87635	[107 94 108]	

J Phys Chem C Nanomater Interfaces. Author manuscript; available in PMC 2020 May 09.

Table 2.

Comparisons between G and A as Traps (Overhangs) in the Hybrid Nanopore

	origami sheet with G overhangs			origami sheet with A overhangs		
parameter	**G2**	**G4**	**GS (G-strip)**	**A-2**	**A-4**	**AS (A-strip)**
mean translocation time (ns)	12.09	55.43	108.21	10.34	28.611	15.67
mean number of hydrogen bonds per ns	4.54	33.55	42.57	0	8.75	6.71

J Phys Chem C Nanomater Interfaces. Author manuscript; available in PMC 2020 May 09.